

Quintessence versus phantom dark energy: the arbitrating power of current and future observations

B. Novosyadlyj¹, O. Sergijenko¹, R. Durrer², V. Pelykh³

January 7, 2013

¹Astronomical Observatory of Ivan Franko National University of Lviv

²Université de Genève, Département de Physique Théorique and CAP

³Ya. S. Pidstryhach Institute for Applied Problems of Mechanics and Mathematics

We analyze the possibility to distinguish between quintessence and phantom scalar field models of dark energy using observations of luminosity distance moduli of SNe Ia, CMB anisotropies and polarization, matter density perturbations and baryon acoustic oscillations. None of the present observations can decide between quintessence or phantom scalar field models at a statistically significant level: for each model a set of best-fit parameters exists, which matches all data with similar goodness of fit. We compare the relative differences of best-fit model predictions with observational uncertainties for each type of data and we show that the accuracy of SNe Ia luminosity distance data is far from the one necessary to distinguish these types of dark energy models, while the CMB data (WMAP, SPT and Planck) are close to being able to distinguish them. Also a significant improvement of the large-scale structure data (e.g. Euclid or BigBOSS) will enable us to decide between quintessence and phantom dark energy.

Introduction

Scalar field models of dark energy are among the most promising and best elaborated ones to match observations of the accelerated expansion of the Universe. This is reflected in the numerous papers, reviews and text books on the subject (see for example [1, 2, 3, 4, 5, 6, 7, 8, 9, 10, 11] and citing therein). However, despite good agreement of theoretical predictions with modern observational data a number of problems remain unresolved and the prospects for their solution are unclear. Among them is the question whether dark energy is quintessence, phantom, quintom, k-essence or of some other form. For each of these types of dark energy, cosmological best-fit parameters exist, for which the differences of maximum likelihoods are statistically insignificant for the same datasets. The identification of dark energy type is important in order to establish the properties of dark energy in our Universe, its physical nature, its origin and its couplings to other fundamental fields and particles. Without this knowledge, e.g., we cannot predict the future of our Universe.

For example, in the paper [12, 13] we have shown that quintessence models of dark energy with decreasing and increasing equation of state (EoS) parameter (freezing or thawing quintessence) cannot be distinguished by current observations, but could be so by future data.

In the recent papers [14, 15] it has been shown also that some datasets slightly prefer phantom models over quintessence, while in contrary other datasets prefer quintessence. However, in all the cases considered, the differences in the maximum likelihoods are not statistically significant.

The goal of this paper is to estimate the possibility to distinguish between quintessence and phantom scalar field models using the current and future observational data.

1 Scalar field dark energy and best-fit cosmological models

We suppose that our Universe is spatially flat and filled with the non-relativistic particles (cold dark matter and baryons), relativistic particles (the thermal cosmic microwave background (CMB) and massless neutrino) and a minimally coupled scalar field with given Lagrangian. The scalar field is specified as follows: (i) its Lagrangian is canonical, $L_{de} = \pm X - U(\phi)$ ($X = \dot{\phi}^2/2$ is the kinetic term and $U(\phi)$ is the potential), with “+” for a quintessence scalar field (QSF) and “-” for a phantom scalar field (PSF). The effective sound speed $c_{s(de)}^2 \equiv \delta p_{de}/\delta \rho_{de}$ (speed of propagation of the scalar field perturbations) is equal to the speed of light c for both cases; (ii) its equation of state is $p_{de} = w_{de} c^2 \rho_{de}$ and the time derivative of the dark energy pressure is proportional to the time derivative of its energy density, $\dot{p}_{de} = c_a^2 c^2 \dot{\rho}_{de}$. The coefficient c_a^2 , often called “squared adiabatic sound speed”¹, is constant. Integrating this equation we obtain the generalized linear barotropic equation of state $p_{de} = c_a^2 \rho_{de} + C$, where C is a constant, that is why we call such scalar field barotropic.

We solve Einstein’s equations for the background dynamics and the Einstein-Boltzmann system of linear perturbation equations in the synchronous gauge for the evolution of the perturbations. The background Universe is assumed to be the spatially flat homogeneous and isotropic with Friedmann-Robertson-Walker (FRW) metric, $ds^2 = g_{ij} dx^i dx^j = a^2(\eta)(d\eta^2 - \delta_{\alpha\beta} dx^\alpha dx^\beta)$, where η is conformal time defined by $cdt = a(\eta)d\eta$ and $a(\eta)$ is the scale factor, normalized to 1 today (below we set $c = 1$). We assume that dark energy and dark matter do not interact. The energy-momentum conservation for dark energy then determines w_{de} and ρ_{de} as functions of the scale factor a ,

$$w_{de} = \frac{(1 + c_a^2)(1 + w_0)}{1 + w_0 - (w_0 - c_a^2)a^{3(1+c_a^2)}} - 1, \quad \rho_{de} = \rho_{de}^{(0)} \frac{(1 + w_0)a^{-3(1+c_a^2)} + c_a^2 - w_0}{1 + c_a^2}. \quad (1)$$

Using the Friedmann equations we obtain the Hubble and deceleration parameters

$$H = H_0 \sqrt{\Omega_r a^{-4} + \Omega_m a^{-3} + \Omega_{de} f(a)}, \quad q = \frac{1}{2} \frac{2\Omega_r a^{-4} + \Omega_m a^{-3} + (1 + 3w_{de})\Omega_{de} f(a)}{\Omega_r a^{-4} + \Omega_m a^{-3} + \Omega_{de} f(a)}, \quad (2)$$

where $f(a) = \rho_{de}/\rho_{de}^{(0)}$, $\rho_{de}^{(0)}$ is current value of dark energy density, w_0 is EoS parameter w_{de} today, H_0 is current value of Hubble parameter (Hubble constant) and $\Omega_r \equiv \rho_r^{(0)}/\rho_{tot}^{(0)}$, $\Omega_m \equiv \rho_m^{(0)}/\rho_{tot}^{(0)}$, $\Omega_{de} \equiv \rho_{de}^{(0)}/\rho_{tot}^{(0)}$ are the dimensionless density parameters of the relativistic, non-relativistic and dark energy components correspondingly. The first Friedmann equation requires $\Omega_r + \Omega_m + \Omega_{de} = 1$. The matter density parameter is the sum of cold dark matter and baryons, $\Omega_m \equiv \Omega_{cdm} + \Omega_b$, and $\rho_{tot}^{(0)} \equiv \rho_r^{(0)} + \rho_m^{(0)} + \rho_{de}^{(0)}$.

¹It corresponds only formally to the adiabatic sound speed in thermodynamics.

Since the light neutrinos have become non-relativistic by today, the density parameter of the present relativistic component is given only by the photon density which is accurately determined by the value of the CMB temperature, $\Omega_r = \Omega_\gamma = 16\pi G a_{SB} T_0^4 / 3H_0^2 = 2.49 \cdot 10^{-5} h^{-2}$ and can be neglected in the matter and dark energy dominated epochs. The density parameters of the other components are less well known and depend somewhat on the model of dark energy². The scalar field affects the expansion of the Universe, it causes accelerated expansion when $|(1 + 3w_{de})\Omega_{de}f(a)| > \Omega_m a^{-3}$ as follows from eqs. (2).

Using expressions (1) and (2) we can compute the “luminosity distance - redshift” or “angular diameter distance - redshift” relations to determine all the above-mentioned parameters by comparison with corresponding observational data on standard candles (supernovae type Ia, γ -ray bursts or other) and standard rulers (positions of the CMB acoustic peaks, baryon acoustic oscillations, X-ray gas in clusters or other).

We assume the standard paradigm of large scale structure formation: (i) it is formed from stochastic, adiabatic, Gaussian scalar perturbations generated in the early Universe, (ii) the initial power spectrum of radiation and matter density perturbations is power-law, $P_i(k) = A_s k^{n_s}$, where A_s and n_s are the amplitude and spectral index (k is wave number). The scalar field cannot be perfectly smooth, it is perturbed by gravitational influence of matter-radiation inhomogeneities or has its own initial fluctuations, generated in the early Universe.

The system of linear differential equations for the evolution of quintessence and phantom scalar field perturbations and their numerical solutions are analyzed in our previous papers [14, 16, 17]. The main conclusions are as follows: (i) the amplitude of scalar field density perturbations at any epoch depends strongly on parameters of barotropic scalar field Ω_{de} , w_0 , c_a^2 and c_s^2 ; (ii) although the density perturbations of dark energy at the current epoch are significantly smaller than matter density perturbations, they leave noticeable imprints in the matter power spectrum, which can be used to constrain the scalar field parameters.

The linear power spectrum of each component can be computed by numerical integration of the Einstein-Boltzmann equations [18, 19, 20, 21] using publicly available codes such as CMBFAST [22, 23], CMBEasy [24], CAMB [25, 26] or CLASS [27, 28, 29],

$$P_{lin}(k) = P_i(k) T^2(k; \Omega_r, \Omega_b, \Omega_{cdm}, \Omega_{de}).$$

$T(k)$ is the transfer function, for the cosmological model with the given parameters. In all the computations presented here and in recent papers, we use CAMB with corresponding modifications for the quintessence/phantom barotropic scalar field as dark energy. Comparison of computed matter density power spectra with the ones obtained from galaxy surveys constrains the parameters of the models discussed here.

The same Einstein-Boltzmann equations and codes also determine the angular power spectra of CMB temperature anisotropies, C_ℓ^{TT} , and polarization, C_ℓ^{EE} , as well as their correlations, C_ℓ^{TE} , which can be compared with WMAP data to constrain the cosmological and DE parameters mentioned above. The calculation of CMB anisotropies and polarization requires also the knowledge of the reionization history of the Universe, which depends on complicated non-linear effects of structure formation. This is parameterized by the value of optical depth from current epoch to decoupling (at redshift z_{dec}) caused by Thomson scattering. It is denoted by τ_{dec} and is also fitted by the data. As it is supported by numerous papers (see for example reviews [1, 2, 3, 4, 5, 6, 7, 8, 9, 10, 11] and citing therein), the CMB data are the most important ones in the determination of cosmological parameters. The parameter estimation from the data is performed using publicly available Markov chain Monte Carlo (MCMC) codes [30, 31].

²Here and below $h \equiv H_0/100\text{km/s Mpc}$

Table 1: The best-fit values [14] and approximate 2σ marginalized confidence ranges of cosmological model parameters for QSF (\mathbf{q}) and PSF (\mathbf{p}) determined by the MCMC technique using 2 observational datasets: WMAP7 + HST + BBN + BAO + SN SDSS SALT2 (\mathbf{q}_1 , \mathbf{p}_1) and WMAP7 + HST + BBN + BAO + SN SDSS MLCS2k2 (\mathbf{q}_2 , \mathbf{p}_2). We denote the rescaled energy density of the component X by $\omega_X \equiv \Omega_X h^2$.

Parameters	QSF+CDM	PSF+CDM	QSF+CDM	PSF+CDM
	\mathbf{q}_1	\mathbf{p}_1	\mathbf{q}_2	\mathbf{p}_2
Ω_{de}	$0.730^{+0.022}_{-0.035}$	$0.723^{+0.030}_{-0.027}$	$0.702^{+0.029}_{-0.036}$	$0.692^{+0.040}_{-0.026}$
w_0	$-0.996^{+0.089}_{-0.004}$	$-1.043^{+0.043}_{-0.14}$	$-0.83^{+0.087}_{-0.17}$	$-1.002^{+0.002}_{-0.095}$
c_a^2	$-0.022^{+0.022}_{-0.978}$	$-1.12^{+0.12}_{-0.46}$	$-0.88^{+0.59}_{-0.12}$	$-1.19^{+0.19}_{-0.37}$
$10\omega_b$	$0.226^{+0.011}_{-0.010}$	$0.223^{+0.011}_{-0.009}$	$0.226^{+0.012}_{-0.010}$	$0.223^{+0.010}_{-0.009}$
ω_{cdm}	$0.110^{+0.007}_{-0.009}$	$0.115^{+0.008}_{-0.007}$	$0.108^{+0.011}_{-0.008}$	$0.119^{+0.007}_{-0.008}$
h	$0.702^{+0.019}_{-0.035}$	$0.704^{+0.032}_{-0.021}$	$0.663^{+0.031}_{-0.027}$	$0.678^{+0.035}_{-0.017}$
n_s	$0.974^{+0.025}_{-0.027}$	$0.965^{+0.024}_{-0.024}$	$0.971^{+0.031}_{-0.022}$	$0.965^{+0.020}_{-0.027}$
$\log(10^{10}A_s)$	$3.085^{+0.067}_{-0.071}$	$3.089^{+0.069}_{-0.061}$	$3.069^{+0.084}_{-0.055}$	$3.113^{+0.049}_{-0.078}$
τ_{rei}	$0.091^{+0.024}_{-0.025}$	$0.085^{+0.025}_{-0.021}$	$0.089^{+0.027}_{-0.023}$	$0.086^{+0.021}_{-0.024}$
$-\log L$	3865.01	3864.86	3857.21	3859.30

The cosmological model with quintessence/phantom barotropic scalar field with canonical Lagrangian has 9 free parameters Ω_b , Ω_{cdm} , Ω_{de} , w_0 , c_a^2 , H_0 , A_s , n_s , τ_{dec} in the general case and 8 when we restrict ourselves to spatially flat cosmological models, since $\Omega_b + \Omega_{cdm} + \Omega_{de} = 1$. To constrain these parameters we used the following datasets:

1. CMB temperature fluctuations and polarization angular power spectra from the 7-year WMAP observations (hereafter WMAP7) [32, 33, 34].
2. Baryon acoustic oscillations in the space distribution of galaxies from SDSS DR7 (hereafter BAO) [35];
3. Hubble constant measurements from HST (hereafter HST) [36].
4. Big Bang Nucleosynthesis prior on baryon abundance (hereafter BBN) [37, 38].
5. Supernovae Ia luminosity distances from SDSS compilation (hereafter SN SDSS) [39], determined using SALT2 method of light curve fitting [40] (hereafter SN SDSS SALT2) and MLCS2k2 [41] one (hereafter SN SDSS MLCS2k2).

In our previous paper [14] we have performed the Markov chain Monte Carlo (MCMC) analysis for two combined datasets: WMAP7 + HST + BBN + BAO + SN SDSS SALT2 (dataset 1) and WMAP7 + HST + BBN + BAO + SN SDSS MLCS2k2 (dataset 2) to determine the best-fit values and confidence limits of the model parameters for QSF/PSF. The results are presented in Table 1. The upper/lower limits are approximate marginalized 2σ ranges from the 1D posteriors. In the last row the negative of the logarithms of maximum of likelihood functions, $\chi^2 = -\log(L_{max})$, are shown for comparison. The PSF+CDM model with best-fit parameters

\mathbf{p}_1 determined on the base of dataset 1 has a slightly lower χ^2 than the QSF+CDM model with best-fit parameters \mathbf{q}_1 . In the case of dataset 2 the result is opposite: the QSF+CDM model with best-fit parameters \mathbf{q}_2 matches the dataset 2 better than the PSF+CDM model with best-fit parameters \mathbf{p}_2 .

In Ref. [14] we have also determined the best-fit parameters of Λ CDM from the datasets 1 and 2 and we have found that in both cases the χ^2 for Λ CDM is between the corresponding values for QSF+CDM and PSF+CDM. This trend suggests that the best-fit parameters of QSF+CDM and PSF+CDM (except for c_a^2) are determined reliably. But in both cases the differences of the χ^2 's are not statistically significant. Hence, we have a degeneracy between the QSF and PSF models of dark energy and we shall elucidate here how strong this degeneracy is and whether the accuracy of current or forthcoming data is sufficient for lift it. Observational constraints for another class of scalar fields with barotropic equation of state without peculiarities in the past are discussed in Appendix A.

The results for the cosmological parameters, especially H_0 , Ω_{de} , w_{de} and c_a^2 , presented in Table 1, also indicate a tension between the two fitters SALT2 and MLCS2k2 applied to the same SNe Ia. This has already been highlighted and analyzed in Refs. [39, 42], but up to now we have no decisive arguments for favor of one of the two lightcurve fitters.

2 Distinguishing quintessence and phantom field models of dark energy

The QSF+CDM model with best-fit parameters \mathbf{q}_i and PSF+CDM model with best-fit parameters \mathbf{p}_i all provide a good fit to the data from SNe Ia distance moduli (left panel of Fig. 1), BAOs (left panel of Fig. 3), matter power spectrum (left panel of Fig. 4), CMB temperature fluctuations, polarization and cross-correlations polarization (left panel of Fig. 5). Let us analyze the possibility to distinguish between QSF+CDM and PSF+CDM by each type of data.

The lines corresponding to different DE models in the left panel of Fig. 1 look perfectly superimposed. The maximal values of relative differences of SNe Ia distance moduli ($|\mu(\mathbf{q}_i) - \mu(\mathbf{p}_i)|/\mu(\mathbf{q}_i)$) for QSF+CDM and PSF+CDM models with best-fit parameters determined using the same fitters are less than 0.1% (right panel of Fig.1). Comparing this to the observational uncertainties plotted as dots and triangles, we conclude that these data are very far from distinguishing between the proposed types of scalar field dark energy.

Fortunately, other characteristics of the expansion dynamics of the Universe, based on measurements of the first and second time derivatives of the Hubble parameter³ $H(z)$, are significantly more sensitive to the current value and time dependence of the EoS parameter. The redshift dependence of dimensionless parameters describing the expansion dynamics of the Universe, such as the rate of expansion H/H_0 , the deceleration parameter $q = -\dot{H}/(aH^2) - 1$ and the statefinder parameters [43]

$$r = \ddot{H}/(a^2 H^3) + 2\dot{H}/(aH^2) + 1, \quad s \equiv (r - 1)/3(q - 1/2), \quad (3)$$

are shown in Fig. 2 for the models with best-fit parameters \mathbf{q}_1 , \mathbf{q}_2 , \mathbf{p}_1 and \mathbf{p}_2 . In our dark

³ $\mu(z) \equiv m - M = 5 \log d_L + 25$ is the integral of $1/H$ over redshift, since $d_L(z) = (1+z)c \int_0^z dz'/H(z')$; $H(z)$ can be deduced from observations by differentiating of $\mu(z)$ with respect to z , since $H(z) = \left[\frac{d}{dz} \left(\frac{d_L}{z+1} \right) \right]^{-1}$.

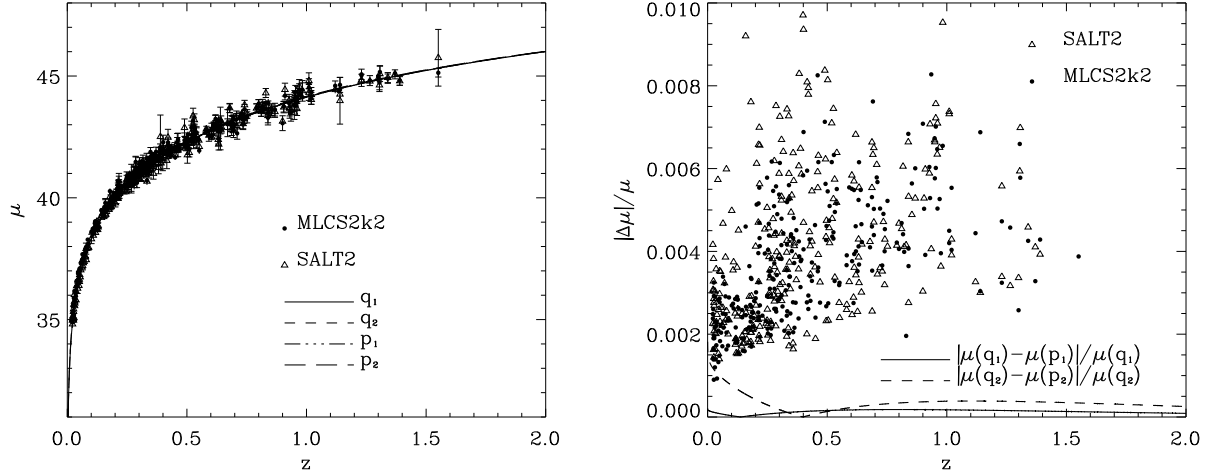


Figure 1: Left panel: the distance modulus $\mu \equiv m - M$ as function of the redshift z for SNe Ia in the models with best-fit parameters \mathbf{q}_1 , \mathbf{q}_2 , \mathbf{p}_1 and \mathbf{p}_2 (superimposed lines) are compared to the data from SDSS SNe Ia (symbols). Right panel: the relative differences of distance moduli in QSF+CDM and PSF+CDM with best-fit parameters determined from the same datasets (lines) are compared with observational uncertainties for SDSS SNe Ia (symbols).

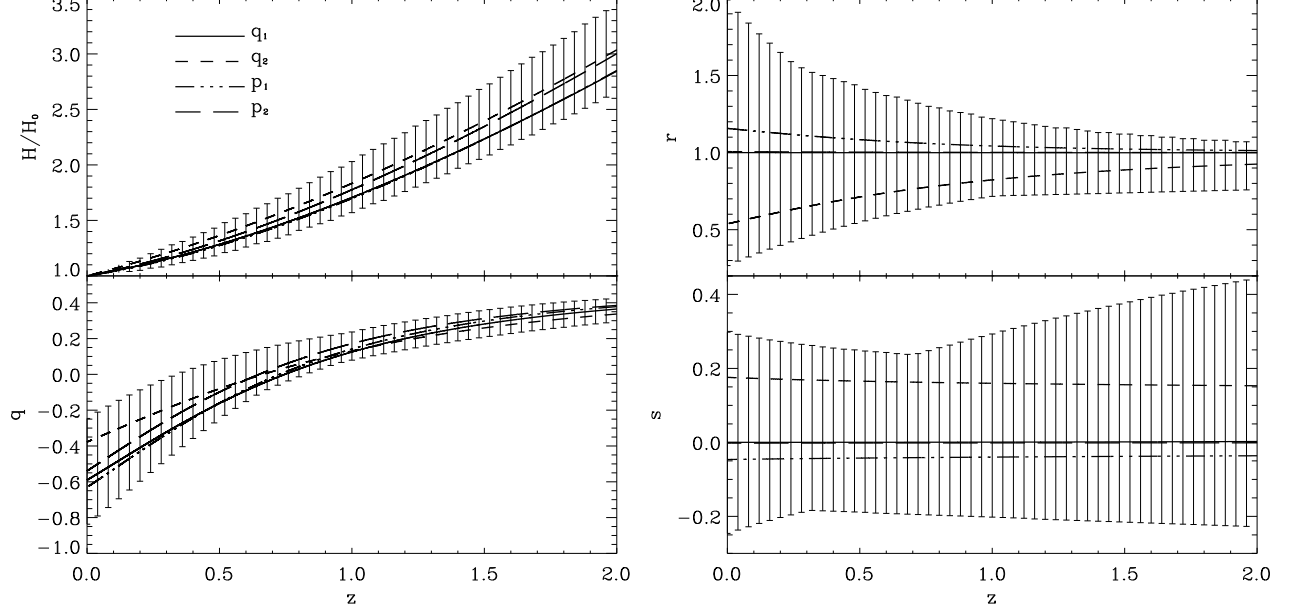


Figure 2: The redshift dependence of dimensionless parameters describing the expansion dynamics of the Universe for the models with best-fit parameters \mathbf{q}_1 , \mathbf{q}_2 , \mathbf{p}_1 and \mathbf{p}_2 . The rate of expansion H/H_0 (left panel, top), the deceleration parameter q (left panel, bottom) and the statefinder parameters r and s (right panel) are shown. The dashed ranges are their observational uncertainties estimated by variation of the expressions (2) for H/H_0 , q , (4) for r and s over Ω_{de} , w_0 , c_a^2 for 2σ marginalized uncertainties of all models presented in Table 1.

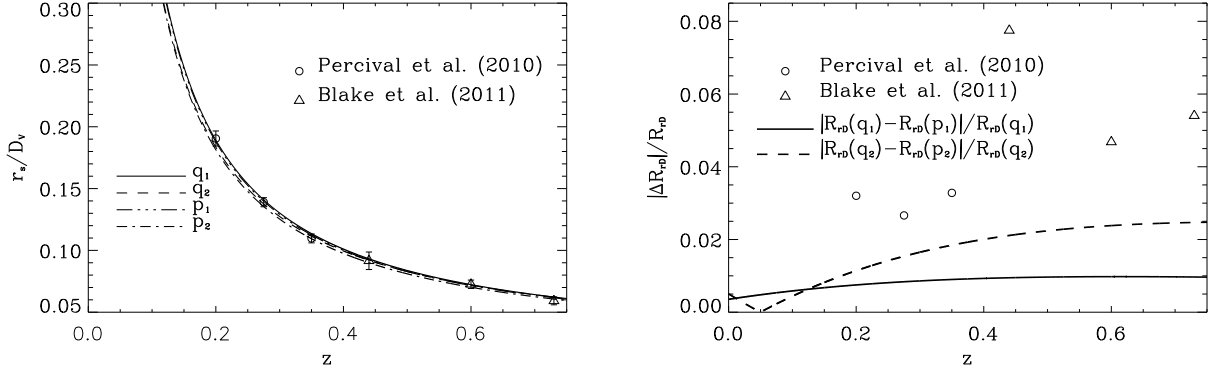


Figure 3: Left panel: the relative BAO distance measure $R_{rD} \equiv r_s(z_{\text{drag}})/D_V(z)$ for the models with best-fit parameters \mathbf{q}_1 , \mathbf{q}_2 , \mathbf{p}_1 and \mathbf{p}_2 (lines) is compared with data from the SDSS DR7 [35] and WiggleZ [44] surveys (symbols). Right panel: the relative differences of the BAO distance measure $|\Delta R_{rD}|/R_{rD}$ in the models with best-fit parameters \mathbf{q}_i and \mathbf{p}_i . Symbols show observational 1σ errors of the data in the left panel.

energy models (1) the state finder parameters reduce to

$$r = 1 + 4.5(1 + w_{de})c_a^2\Omega_{de}(a), \quad s = (1 + w_{de})c_a^2/w_{de}, \quad (4)$$

where $\Omega_{de}(a) \equiv 8\pi G\rho_{de}(a)/3H^2$. The differences between H/H_0 for \mathbf{q}_i and \mathbf{p}_i , as well as between $q(\mathbf{q}_i)$ and $q(\mathbf{p}_i)$, $s(\mathbf{q}_i)$ and $s(\mathbf{p}_i)$, $r(\mathbf{q}_i)$ and $r(\mathbf{p}_i)$, at different z are significantly larger than those of $\mu(z)$ or $d_L(z)$. Unfortunately, current data on $d_L(z)$ from SN Ia measurements are too poor to determine these quantities. The dashed ranges in Fig. 2 show the dispersion obtained by the variation of expressions (2) for H/H_0 and q , (4) for r and s over Ω_{de} , w_0 , c_a^2 within the 2σ uncertainties of all models presented in Table 1. Maybe future high-precision measurements of distances to a significantly larger number of SN Ia or extremely well-calibrated γ -ray bursts will provide a possibility to distinguish the QSF and PSF models of DE. But clearly, present SNe Ia data is very far from this goal.

The relative BAO distance measure $R_{rD}(z) \equiv r_s(z_{\text{drag}})/D_V(z)$ ($r_s(z_{\text{drag}})$ is the sound horizon at the epoch where photon drag stops due to recombination and $D_V(z)$ is the BAO dilation scale) extracted from SDSS DR7 galaxy redshift survey [35] and from the WiggleZ survey [44] is matched well by the QSF+CDM and PSF+CDM models with best-fit parameters \mathbf{q}_1 , \mathbf{q}_2 , \mathbf{p}_1 and \mathbf{p}_2 (see Fig. 3, left panel). The relative differences of $R_{rD}(z)$ for models with QSF and PSF are up to 2% for $z \leq 0.4$, while observational errors are about 3% at $0.2 \leq z \leq 0.35$ and more than 4.5% at $0.44 \leq z \leq 0.73$ (right panel of Fig. 3). This means that an improvement by a factor 2 to 3 in the determination of $R_{rD}(z)$ in future large scale structure surveys like BigBOSS [45] or Euclid [46] can distinguish between these types of dark energy. The power spectrum of matter density perturbations extracted from luminous red galaxies sample from SDSS DR7 catalogue by Reid et al. (2010) [47] has not been used for the determination of best-fit parameters of QSF+CDM and PSF+CDM, however the computed power spectra match it well too. The experimental errors of its determination are still too large (8–12%) to distinguish between different scalar field models of dark energy. In addition, at the small scales ($k \geq 0.1 \text{ hMpc}^{-1}$) there are uncertainties in the computation of the power spectrum associated with the nonlinear evolution of perturbations. The resolution of this problem would require combined N-body + scalar field simulations.

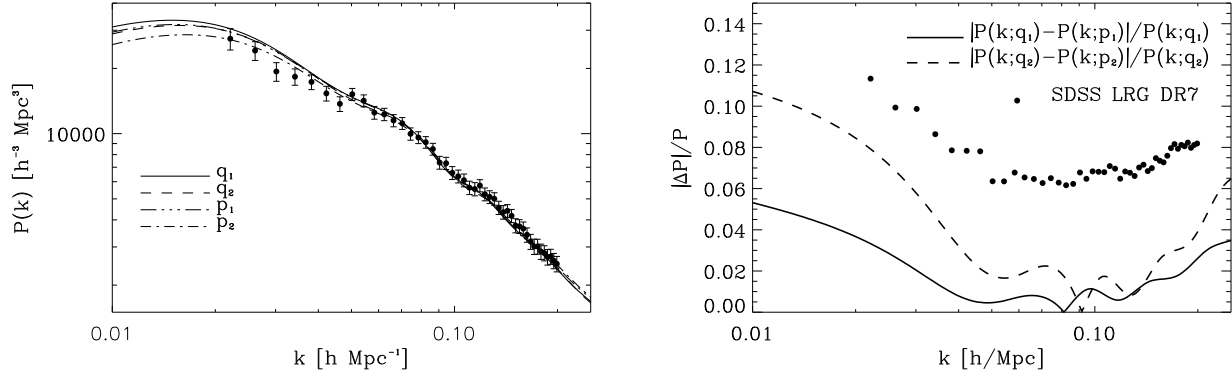


Figure 4: Left panel: the power spectrum of matter density perturbations in the cosmological models with best-fit parameters \mathbf{q}_1 , \mathbf{q}_2 , \mathbf{p}_1 and \mathbf{p}_2 . Dots show the observational SDSS LRG DR7 power spectrum [47]. Right panel: the relative differences of matter density power spectra $|\Delta P(k)|/P(k)$ in the models with best-fit parameters \mathbf{q}_i and \mathbf{p}_i . The dots show the observational uncertainties (1σ) of SDSS LRG DR7 data [47].

Above we have discussed the importance of CMB data for the determination of cosmological parameters and, in particular, for dark energy parameters. The key cosmological data at present are the WMAP all-sky maps, which contain information about the primordial fluctuation amplitude and spectral index, the positions and amplitudes of the acoustic peaks, as well as the amplitude of large scale matter density perturbations at late time imprinted on the integrated Sachs-Wolfe effect. In Fig. 5 (top left panel) the power spectra of temperature fluctuations extracted from the 7-year [32, 33, 34] and 9-year [48, 49] WMAP all-sky measurements are shown. Its accuracy is best (minimal errors $\sim 1.5 - 4\%$) in the range of the first and second acoustic peaks ($\ell \sim 200 - 600$). This allows an accurate determination of the main cosmological parameters. The best accuracy of dark energy parameters is achieved when CMB data are used together with SNe Ia data and relative BAO distance measures or directly the matter power spectrum. The power spectra $\ell(\ell+1)C_\ell^{TT}/2\pi$ for the QSF+CDM and PSF+CDM models with best-fit parameters \mathbf{q}_1 , \mathbf{q}_2 , \mathbf{p}_1 and \mathbf{p}_2 provide good fits to the WMAP7 and WMAP9 data, as well as to other recent CMB experiments, ACT [50] and SPT [51], which are sensitive to higher values of ℓ . The relative differences between the power spectra in QSF+CDM and PSF+CDM models, shown in the top right panel of Fig. 5, do not exceed the relative observational uncertainties of $\ell(\ell+1)C_\ell^{TT}/2\pi$ for ACT. The relative difference between the spectra in models with parameters \mathbf{q}_2 and \mathbf{p}_2 is comparable to the relative uncertainties of WMAP7 and especially WMAP9 data at $\ell \sim 300 - 800$ and to the relative uncertainties of SPT data at higher ℓ .

We also present the forecasted uncertainties of the Planck data (based on the sensitivities for 7 frequency channels which can measure the polarization [52], f_{sky} is taken to be 0.65). For $\ell < 500$, the WMAP errors are already nearly cosmic variance limited and the Planck data will not bring a significant improvement. At high ℓ , however, the forecasted Planck uncertainties are smaller (for \mathbf{q}_2 and \mathbf{p}_2) or comparable (for \mathbf{q}_1 and \mathbf{p}_1) to the relative differences of models. This is in good agreement with our previous conclusion [12, 13] that the accuracy of the power spectra expected from Planck will significantly narrow the allowed range of parameter values for scalar field models of dark energy.

Additional constraints on cosmological parameters are obtained when CMB polarization data are included. To illustrate the agreement between theory and observations, the temperature-

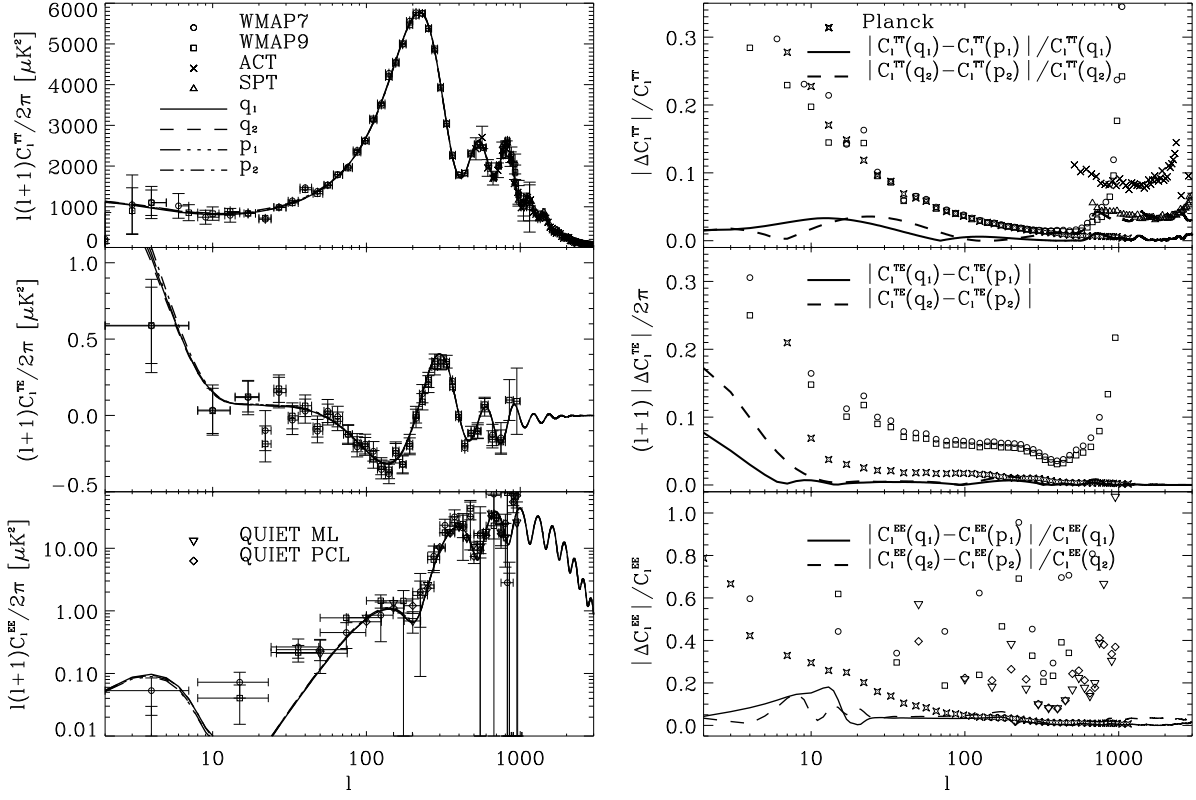


Figure 5: Left panel: the temperature (TT), temperature-polarization (TE) and polarization (EE) CMB angular power spectra, $\ell(\ell+1)C_\ell^{TT}/2\pi$, $(\ell+1)C_\ell^{TE}/2\pi$ and $\ell(\ell+1)C_\ell^{EE}/2\pi$, for the cosmological models with best-fit parameters \mathbf{q}_1 , \mathbf{q}_2 , \mathbf{p}_1 and \mathbf{p}_2 (superimposed lines) are compared to currently available data (symbols). Right panel: the relative differences of temperature $|\Delta C_\ell^{TT}|/C_\ell^{TT}$ and polarization $|\Delta C_\ell^{EE}|/C_\ell^{EE}$ power spectra and absolute differences for the temperature-polarization correlation, $(\ell+1)|\Delta C_\ell^{TE}|/2\pi$, in the models with best-fit parameters \mathbf{q}_i and \mathbf{p}_i (Table 1). The symbols show 1σ uncertainties of currently available and forecasted future data.

polarization $(\ell+1)C_\ell^{TE}/2\pi$ and polarization $\ell(\ell+1)C_\ell^{EE}/2\pi$ CMB power spectra for the cosmological models with best-fit parameters \mathbf{q}_1 , \mathbf{q}_2 , \mathbf{p}_1 and \mathbf{p}_2 are presented in the middle and bottom left panels of Fig. 5. All lines are superimposed for $\ell > 20$ with sub-percent accuracy for TE and a few percents for EE, while the errors of the WMAP7 and WMAP9 power spectra at these ℓ 's are larger than $\sim 3 - 6\%$ for TE and $\sim 20 - 40\%$ for EE, as it is shown in the middle and bottom right panels of Fig. 5. In the bottom right panel of Fig. 5 we present also the relative uncertainties from the QUIET experiment [53] (for both maximal likelihood and pseudo- C_ℓ s). The minimal errors of the QUIET EE power spectra at high ℓ are at least $\sim 10 - 20\%$. The forecasted relative uncertainties for Planck are comparable to the differences between the models at high ℓ . All this means that the data on polarization of CMB are insufficient for the problem of distinguishing between quintessence and phantom fields at the present level of accuracy of observational data, but will possibly become sufficient in near future.

3 Conclusion

None of the used observational data at the current level of accuracy can prefer quintessence cosmology (QSF + CDM) or phantom cosmology (PSF + CDM) at a statistically significant level. In the framework of each model a set of best-fit parameters exists. The best-fit model matches well each type of data and all together with similar goodness of fit. At present, the data on CMB temperature fluctuations from WMAP9 and SPT and the expected Planck data look most promising for the purpose of distinguishing between these models of dark energy. In the future, increasing the accuracy of CMB fluctuation measurements jointly with high precision matter density data will probably give the possibility to establish the dynamical properties of dark energy and, maybe, its nature. On the other hand, SNe Ia luminosity distance measurements do not seem very promising.

Acknowledgments

This work was supported by the project of Ministry of Education and Science of Ukraine (state registration number 0110U001385), research program “Cosmomicrophysics” of the National Academy of Sciences of Ukraine (state registration number 0109U003207) and the SCOPES project No. IZ73Z0128040 of Swiss National Science Foundation. Authors also acknowledge the usage of CAMB and CosmoMC packages.

A Observational constraints on scalar field models with $w_0 > -1$, $c_a^2 < -1$

Another subclass of scalar field models of dark energy with barotropic equation of state without peculiarities in the past are fields with $w_0 > -1$, $c_a^2 < -1$. In the past the EoS parameter of such fields evolved from -1 at early epoch to w_0 today. The properties of these models will be studied in detail in a separate paper, here we only present observational constraints on them from the datasets 1 and 2, determined by the MCMC technique in the same way as in [14].

In Fig. 6 we see that while for w_0 the posteriors and mean the likelihoods are close and have the shape of Gaussian and half-Gaussian, for c_a^2 the shapes of the likelihoods differ significantly from each other and from Gaussian. This means that also for such fields the range of acceptable values of c_a^2 is generally unconstrained (it is constrained only in the case \mathbf{q}_2). The ranges of acceptable values of all other parameters of the models studied here including w_0 are well constrained. In Table 2 we present the best-fit values and approximate 2σ marginalized confidence ranges of cosmological parameters in models with scalar fields with $w_0 > -1$, $c_a^2 < -1$. The value of χ^2 for this model in case of dataset 1 is larger than the corresponding value for both quintessence and phantom dark energy. On the other hand, for the dataset 2 the value of χ^2 is smaller than for the quintessence and phantom models. Thus the scalar field with $w_0 > -1$, $c_a^2 < -1$ is preferred by the dataset 2, however, again the difference is not statistically significant.

Comparing the relative differences of distance moduli, BAO relative distance measures, matter density perturbations and CMB power spectra between such models and either quintessence or phantom we see that scalar fields with $w_0 > -1$, $c_a^2 < -1$ could only become distinguished from them in near future by Planck data. The probability of distinguishing them from phantom

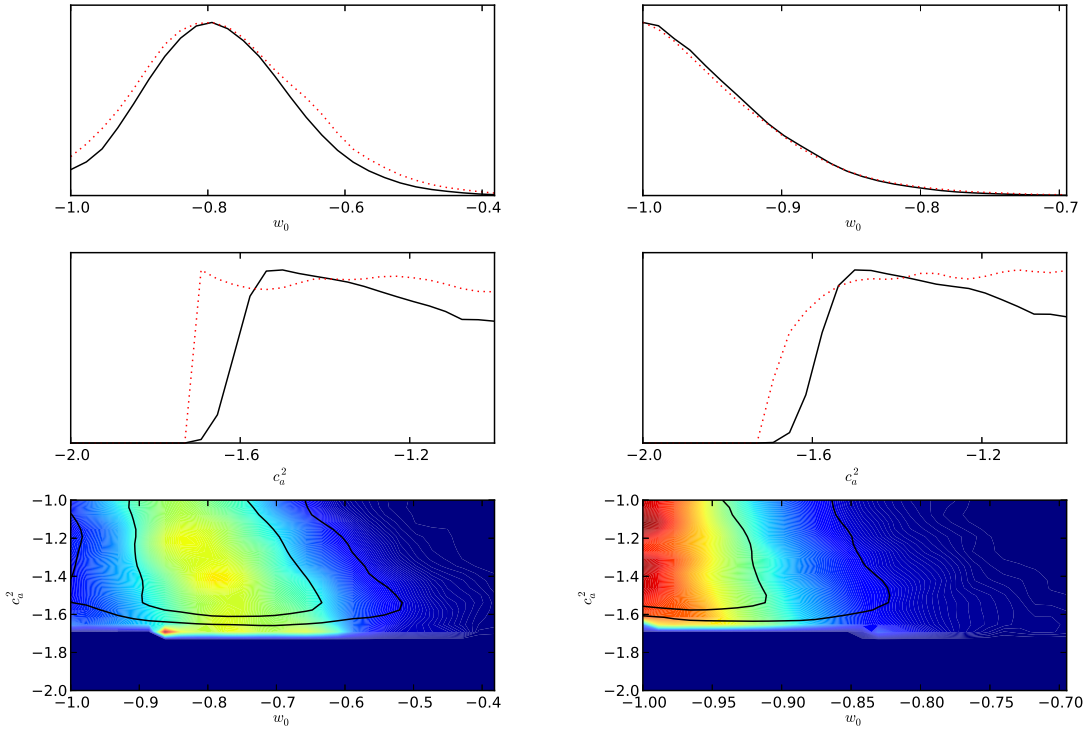


Figure 6: One-dimensional marginalized posteriors (solid lines) and mean likelihoods (dotted lines) for w_0 (top panels) and c_a^2 (middle panels) in models with $w_0 > -1$, $c_a^2 < -1$. Left: WMAP7 + HST + BBN + BAO + SN SDSS MLCS2k2. Right: WMAP7 + HST + BBN + BAO + SN SDSS SALT2. Bottom: the corresponding two-dimensional mean likelihood distributions in the plane $c_a^2 - w_0$. Solid lines show the 1σ and 2σ confidence contours.

fields is slightly higher than from quintessence ones. At current level of accuracy the models are indistinguishable by all data.

References

- [1] Copeland E.J., Sami M., Tsujikawa S., *Dynamics of Dark Energy*, *Int. J. Mod. Phys. D* **15** (2006) 1753.
- [2] Turner M.S., Huterer D., *Cosmic Acceleration, Dark Energy and Fundamental Physics*, *J. Phys. Soc. Jap.* **76** (2007) 111015.
- [3] Special issue on dark energy, Eds. G. Ellis, H. Nicolai, R. Durrer, R. Maartens, *Gen. Relat. Gravit.* **40** (2008).
- [4] Frieman J.A., Turner M.S., Huterer D., *Dark Energy and the Accelerating Universe*, *Ann. Rev. Astron. Astrophys.* **46** (2008) 385.
- [5] Lukash V.N., Rubakov V.A., *Dark energy: myths and reality*, *Phys. Uspekhi* **51** (2008) 283.

Table 2: The best-fit values and approximate 2σ marginalized confidence ranges for parameters of cosmological models with scalar fields with $w_0 > -1$, $c_a^2 < -1$ determined by the MCMC technique using two observational datasets: WMAP7 + HST + BBN + BAO + SN SDSS SALT2 and WMAP7 + HST + BBN + BAO + SN SDSS MLCS2k2. The rescaled energy density of the component X is denoted by $\omega_X \equiv \Omega_X h^2$.

Parameter	MLCS2k2	SALT2
Ω_{de}	$0.700^{+0.030}_{-0.035}$	$0.727^{+0.025}_{-0.031}$
w_0	$-0.849^{+0.256}_{-0.087}$	$-0.987^{+0.145}_{-0.013}$
c_a^2	$-1.073^{+0.073}_{-0.515}$	$-1.481^{+0.481}_{-0.084}$
$10\omega_b$	$0.226^{+0.012}_{-0.009}$	$0.224^{+0.012}_{-0.009}$
ω_{cdm}	$0.111^{+0.008}_{-0.009}$	$0.112^{+0.006}_{-0.008}$
h	$0.668^{+0.027}_{-0.030}$	$0.701^{+0.021}_{-0.031}$
n_s	$0.972^{+0.027}_{-0.024}$	$0.968^{+0.028}_{-0.021}$
$\log(10^{10} A_s)$	$3.086^{+0.067}_{-0.068}$	$3.084^{+0.069}_{-0.068}$
τ_{rei}	$0.090^{+0.025}_{-0.023}$	$0.087^{+0.027}_{-0.021}$
$-\log L$	3857.09	3865.05

- [6] Caldwell R.R., Kamionkowski M., *The Physics of Cosmic Acceleration*, *Ann. Rev. Nucl. Part. Sc.* **59** (2009) 397.
- [7] Cai Y.-F., Saridakis E.N., Setare M. R., Xia J.-Q., *Quintom cosmology: Theoretical implications and observations*, *Phys. Rep.* **493** (2010) 1.
- [8] Blanchard A., *Evidence for the fifth element*, *Astron. Astroph. Rev.* **18** (2010) 595.
- [9] Sapone D., *Dark Energy in Practice*, *Int. J. Mod. Phys. A* **25** (2010) 5253.
- [10] Amendola L. and Tsujikawa S., *Dark Energy: theory and observations*, Cambridge University Press, 507 p. (2010).
- [11] Lectures on Cosmology: Accelerated expansion of the Universe. *Lect. Notes in Physics* **800**, Ed. G. Wolschin, Springer, Berlin–Heidelberg, 188 p. (2010).
- [12] Novosyadlyj B., Sergijenko O., Apunevych S., *Distinguishability of scalar field models of dark energy with time variable equation of state parameter*, *J. Phys. Stud.* **15** (2011) 1901.
- [13] Sergijenko O., Durrer R., Novosyadlyj B., *Observational constraints on scalar field models of dark energy with barotropic equation of state*, *J. Cosmol. Astropart. Phys.* **08** (2011) 004.
- [14] Novosyadlyj B., Sergijenko O., Durrer R., Pelykh V., *Do the cosmological observational data prefer phantom dark energy?* *Phys. Rev. D* **86** (2012) 083008.
- [15] Wang P.-Y., Chen C.-W., Chen P., *Confronting Phantom Dark Energy with Observations*, arXiv:1208.6579.

- [16] Novosyadlyj B., Sergijenko O., *Evolution of scalar perturbations in cosmology with quintessential dark energy*, *J. Phys. Stud.* **13** (2009) 1902.
- [17] Novosyadlyj B., Sergijenko O., Apunevych S., Pelykh V., *Properties and uncertainties of scalar field models of dark energy with barotropic equation of state*, *Phys. Rev. D* **82** (2010) 103008.
- [18] Ma C.-P., Bertschinger E., *Cosmological perturbation theory in the synchronous and conformal newtonian gauges*, *Astrophys. J.* **455** (1995) 7.
- [19] Durrer R., *The theory of CMB anisotropies*, *J. Phys. Stud.* **5** (2001) 177.
- [20] Novosyadlyj B., *The large scale structure of the Universe: theory and observations*, *J. Phys. Stud.* **11** (2007) 226.
- [21] Durrer R., *The Cosmic Microwave Background*, Cambridge University Press, 415 p. (2008).
- [22] Seljak U., Zaldarriaga M., *A Line-of-Sight Integration Approach to Cosmic Microwave Background Anisotropies*, *Astrophys. J.* **469** (1996) 437.
- [23] Zaldarriaga M., Seljak U., *CMBFAST for Spatially Closed Universes*, *Astrophys. J. Suppl.* **129** (2000) 431.
- [24] Doran M., *CMBEASY: an object oriented code for the cosmic microwave background*, *J. Cosmol. Astropart. Phys.* **10** (2005) 011.
- [25] Lewis A., Challinor A., Lasenby A., *Efficient Computation of Cosmic Microwave Background Anisotropies in Closed Friedmann-Robertson-Walker Models*, *Astrophys. J.* **538** (2000) 473.
- [26] <http://camb.info>
- [27] Lesgourgues J., *The Cosmic Linear Anisotropy Solving System (CLASS) I: Overview*, arXiv:1104.2932
- [28] Blas D., Lesgourgues J., Tram T., *The Cosmic Linear Anisotropy Solving System (CLASS). Part II: Approximation schemes*, *J. Cosmol. Astropart. Phys.* **07** (2011) 034.
- [29] <http://lesgourg.web.cern.ch/lesgourg/class.php>
- [30] Lewis A., Bridle S., *Cosmological parameters from CMB and other data: A Monte Carlo approach*, *Phys. Rev. D* **66** (2002) 103511.
- [31] <http://cosmologist.info/cosmomc>
- [32] Jarosik N., Bennett C.L., Dunkley J. et.al., *Seven-Year Wilkinson Microwave Anisotropy Probe (WMAP) Observations: Sky Maps, Systematic Errors, and Basic Results*, *Astrophys. J. Suppl.* **192** (2011) 14.
- [33] Komatsu E., Smith K.M., Dunkley J. et.al., *Seven-Year Wilkinson Microwave Anisotropy Probe (WMAP) Observations: Cosmological Interpretation*, *Astrophys. J. Suppl.* **192** (2011) 18.

- [34] Larson D., Dunkley J., Hinshaw G. et al., *Seven-year Wilkinson Microwave Anisotropy Probe (WMAP) Observations: Power Spectra and WMAP-derived Parameters*, *Astrophys. J. Suppl.* **192** (2011) 16.
- [35] Percival W.J., Reid B.A., Eisenstein D.J. et al., *Baryon acoustic oscillations in the Sloan Digital Sky Survey Data Release 7 galaxy sample*, *MNRAS* **401** (2010) 2148.
- [36] Riess A.G., Macri L., Casertano S. et al., *A Redetermination of the Hubble Constant with the Hubble Space Telescope from a Differential Distance Ladder*, *Astrophys. J.* **699** (2009) 539.
- [37] Steigman G., *Primordial Nucleosynthesis in the Precision Cosmology Era*, *Ann. Rev. Nucl. Part. Phys.* **57** (2007) 463.
- [38] Wright E.L., *Constraints on Dark Energy from Supernovae, Gamma-Ray Bursts, Acoustic Oscillations, Nucleosynthesis, Large-Scale Structure and the Hubble Constant*, *Astrophys. J.* **664** (2007) 633.
- [39] Kessler R., Becker A.C., Cinabro D. et al., *First-Year Sloan Digital Sky Survey-II Supernova Results: Hubble Diagram and Cosmological Parameters*, *Astrophys. J. Suppl.* **185** (2009) 32.
- [40] Guy J., Astier P., Baumont S. et al., *SALT2: using distant supernovae to improve the use of type Ia supernovae as distance indicators*, *Astron. Astrophys.* **466** (2007) 11.
- [41] Jha S., Riess A.G., Kirshner R.P., *Improved Distances to Type Ia Supernovae with Multi-color Light-Curve Shapes: MLC2k2*, *Astrophys. J.* **659** (2007) 122.
- [42] Bengochea G.R., *Supernova light-curve fitters and dark energy*, *Phys. Lett. B* **696** (2011) 5.
- [43] Sahni V., Saini T.D., Starobinsky A.A., Alam U., *Statefinder – a new geometrical diagnostic of dark energy*, *JETP Lett.* **77** (2003) 201.
- [44] Blake C., Kazin E., Beutler F. et al., *The WiggleZ Dark Energy Survey: mapping the distance-redshift relation with baryon acoustic oscillations*, *MNRAS* **418** (2011) 1707.
- [45] See BigBOSS webpage, <http://bigboss.lbl.gov/>
- [46] Laureijs R. et al., *Euclid Definition Study Report*, arXiv:1110.3193 and Euclid webpage, <http://www.euclid-ec.org>
- [47] Reid B.A., Percival W.J., Eisenstein D.J. et al., *Cosmological constraints from the clustering of the Sloan Digital Sky Survey DR7 luminous red galaxies*, *MNRAS* **404** (2010) 60.
- [48] Bennett C.L., Larson D., Weiland J.L. et al., *Nine-Year Wilkinson Microwave Anisotropy Probe (WMAP) Observations: Final Maps and Results*, arXiv:1212.5225.
- [49] Hinshaw G., Larson D., Komatsu E. et al., *Nine-Year Wilkinson Microwave Anisotropy Probe (WMAP) Observations: Cosmological Parameter Results*, arXiv:1212.5226.

- [50] Das S., Marriage T.A., Ade P.A.R. et al., *The Atacama Cosmology Telescope: A Measurement of the Cosmic Microwave Background Power Spectrum at 148 and 218 GHz from the 2008 Southern Survey*, *Astrophys. J.* **729** (2011) 62.
- [51] Keisler R., Reichardt C.L., Aird K.A. et al., *A Measurement of the Damping Tail of the Cosmic Microwave Background Power Spectrum with the South Pole Telescope*, *Astrophys. J.* **743** (2011) 28.
- [52] The Scientific Programme of Planck, astro-ph/0604069 and Lesgourgues J., Perotto L., Pastor S., Piat M., *Probing neutrino masses with CMB lensing extraction*, *Phys. Rev. D* **73** (2006) 045021.
- [53] Araujo D., Bischoff C., Brizius A. et al., *Second Season QUIET Observations: Measurements of the CMB Polarization Power Spectrum at 95 GHz*, arXiv:1207.5034.